



The Society shall not be responsible for statements or opinions advanced in papers or discussion at meetings of the Society or of its Divisions or Sections, or printed in its publications. Discussion is printed only if the paper is published in an ASME Journal. Authorization to photocopy for internal or personal use is granted to libraries and other users registered with the Copyright Clearance Center (CCC) provided \$3/article or \$4/page is paid to CCC, 222 Rosewood Dr., Danvers, MA 01923. Requests for special permission or bulk reproduction should be addressed to the ASME Technical Publishing Department.

Copyright © 1998 by ASME

All Rights Reserved

Printed in U.S.A.

EXPERIMENTAL AND NUMERICAL INVESTIGATIONS OF FILM-COOLING EFFECTS ON THE AERODYNAMIC PERFORMANCE OF TRANSONIC TURBINE BLADES

Martin F. Urban, Juergen Hermeler,
Hans-Georg Hosenfeld

Siemens AG, KWU Group,
Muelheim / Germany

1 ABSTRACT

This paper presents results of experimental as well as numerical investigations of the aerodynamic performance of film-cooled transonic turbine blades. Taking into consideration to non-dimensional similarity, the experiments were performed on a cascade test rig using superheated steam as fluid. The investigated blading corresponds to a typical high pressure turbine vane used in the high subsonic regime.

In order to determine the effect of the blown-out cooling fluid on the aerodynamic performance of the cascade, the measurements were performed over a wide range of realistic exit Mach numbers, mass flow rate ratios, coolant injection locations and main-to-coolant flow density ratios.

The paper presents the results of the experimental investigation in the form of outlet angles and loss terms, and compares and discusses these for a number of variations. It was found that below a critical mass flow ratio, the kinetic loss coefficient varies only little with flow rate whereas above this critical flow ratio, the loss coefficient increases rapidly.

A comparison of the different injection locations shows that the suction side is very sensitive with regard to main flow disturbances while injection on the pressure side and the trailing edge only has a small effect of the loss terms. Consideration of different coolant-to-mainstream density ratios clarifies that the influence of this parameter on the loss terms can be neglected.

The paper also addresses a simple numerical code which is based on the „TOTLOS“ model of Hartsel and adapted to the above-mentioned problem, and compares and discusses the results of the experimental and numerical investigations.

2 Nomenclature

c	chord length
c_p	specific heat at constant pressure
F	area
h	enthalpy
k	concentration

l	length
Ma	Mach number
m	mass flow
mfr	mass flow rate
p	pressure
Pr	Prandtl number
R	gas constant
Re	Reynolds number
t	pitch
T	temperature
Tu	turbulence level
v	velocity
x, y, z	axial, pitchwise and spanwise coordinate
α	inlet angle
β	outlet angle
$\bar{\beta}$	pitchwise mass-averaged outlet angle
η	dynamic viscosity
γ	isentropic exponent
λ	thermal conductivity
ρ	density
σ	factor of main mass flow
ζ	kinetic energy loss

subscripts

bi	bitangent
c	coolant flow
c_inl	coolant flow at blade inlet
c_ex	coolant flow at film cooling hole exit
d	design ($Ma_{in}=0.75$, all rows, $mfr_i=1$)
is	isentropic
m	mixed flow of mixing layer
M	mixed-out plane
orig	original turbine
pr	profile
solid	solid
t	total
th	thermodynamic

- 0 inlet
- 1 probe traverse plane
- 2 outlet

3 INTRODUCTION

The development of modern gas turbines and the demand for higher efficiencies has led to fast increasing turbine inlet temperatures. Despite the improvements made in the field of thermal material limits, cooling of the blades is still necessary. The most effective method of cooling the first stages is film cooling. Disturbance of the mainstream flow caused by the penetrating cold jet primarily depends on the mass flow ratio and the ejection location, and also appears to be affected by the coolant-to-mainstream density ratio. There are several studies which all deal with the investigation of the effects of the above-mentioned parameters. Experimental research work by Haller and Camus (1984) shows that the cooling efficiency penalty is not affected by changes in coolant density at a constant blowing rate. Osnaghi et al. (1997) shows that the density ratio only has a small effect on the portion of the coolant fluid but states that the loss terms are almost equal when tests are carried out at the same global momentum flux ratio. By contrast, the results presented by Parvizinia (1996) show that a lower ratio of coolant to mainstream density at an equal mass flow rate leads to enlarged wakes which are apparently due to the lower momentum flux. Studies by Oldfield and Lock (1997) point out that, owing to the effects of the density ratio, correct correlation requires matching of the momentum flux ratio rather than the blowing rate.

The investigation of the effect on the ejection location contains a number of problems. Several publications deal with single row film cooling (Parvizinia, Ito et al.) or full-coverage film cooling (Osnaghi et al.). Single row investigations allow the influence of ejection location to be determined precisely but do not contain information about the interaction effect between different rows. Although these effects are included in full coverage film cooled investigations it is impossible to split the loss into parts caused by the different rows.

This study presents experimental data from a two dimensional cascade of turbine blades. The blades investigated are scaled models of the untwisted first-stage guide vanes of Siemens' Model V84.4 gas turbine designed for an isentropic outlet Mach number of $Ma_{2s}=0.75$. At this design point, the blade is of the full-coverage film cooled type with 17 rows of shaped holes located at the trailing edge as well as on the suction and pressure sides.

Although the problem detailed here is particular to gas turbine applications, the investigations were performed on a test rig with steam as working fluid. Although this test rig had originally been designed for investigations on steam turbine cascades, it is possible to use it for investigations on film cooling effects. Superheated steam is treated as ideal a gas as air, and it is thus possible - by using superheated steam as main and as coolant fluid - to vary the ratio of coolant to mainstream density by changing the temperature ratios. In this way the problem of using different flow media for the main and coolant flow (for example air and CO_2) is eliminated and the results are comparable to those of test rigs where air is used as working fluid. The comparison of the non-dimensional similarity (Section 7.1) demonstrates the transferability of the results.

The coolant support for the model blade was designed for a separate coolant steam supply to each row of cooling holes (except

the showerhead). It was thus possible to examine a single row as well as part or full-coverage film cooling.

This paper also presents a simple numerical code based on the "TOTLOS" model of Hartsel. This numerical code is adapted to the above problem (multi-row or full-coverage film cooling) and it is planned that this code be used for the prediction of the mixing loss of cooling air during the design phase of a turbine. The results of the experiments were used to validate this code.

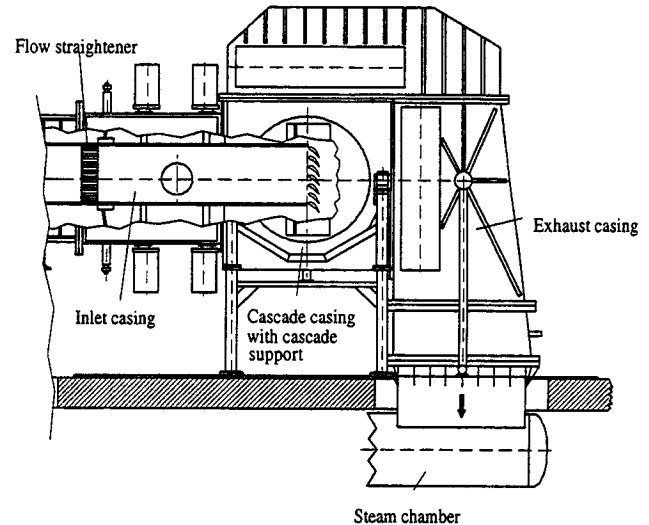


Figure 1: Steam test rig (STR)

4 TEST FACILITY

The steam test rig (STR) at the flow laboratory of Siemens' KWU Group's Mülheim factory was used for the tests (Fig. 1). The test rig is suitable for long-term tests and is supplied with superheated steam from a separate boiler. Table 1 shows the operating parameters of the test rig.

P_{01} :	$= 0.35 \cdot 10^5 \text{ N/m}^2$
T_{01} :	$\approx 520 \text{ K}$
Tu_{01} :	$\leq 1\%$
Ma_2 :	≤ 0.8
Re_2 :	$\leq 4 \cdot 10^5$
m :	$\leq 2.7 \text{ kg/s}$

Table 1: Operating parameters

In order to be able to perform the experiments it was necessary to install a cooling fluid supply. Superheated steam was chosen as coolant because of the non-dimensional similarity and the fact that it can be separated from the main steam. Fig. 2 shows a flow diagram of the test facility. The boiler supplies steam at approx. 430K and $6.0 \cdot 10^5 \text{ N/m}^2$. To ensure superheated steam an electrical heat exchanger heats the steam to a temperature of 520K. A pump reduces the pressure in the test rig to $0.06 \cdot 10^5 \text{ N/m}^2$. The electrical valves at the inlet and outlet of the test rig allow the pressure level to be accurately adjusted. The cooling steam flow is tapped off the main steam downstream of the heat exchanger. Electrically-driven valves and a bypass were installed to enable the pressure of the cooling steam to be controlled, and water

injection provides for regulation of the cooling temperature. Three of the seven blades were provided with cooling steam from a steam plenum. The cooling steam mass flow had to be determined accurately at low flow rates (5-50 g/s) and different specially-designed orifices (15-37.5mm diameter) were used for this purpose.

After leaving the steam test rig, the steam is routed to a condenser from where the condensate is returned to the boiler.

Superheated Steam (6 bar, 430K)

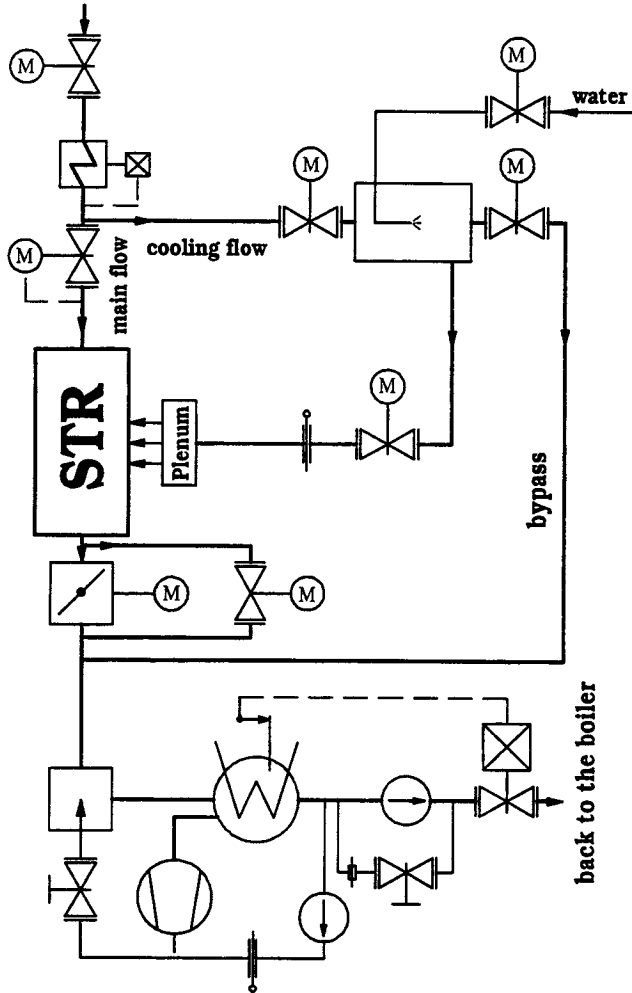


Figure 2: Test facility flow diagram

5 CASCADE GEOMETRY

The cascade consists of 7 blades with a chord length of 123.05 mm (scale factor: 1.2853), a pitch-to-chord length ratio of $t/c=0.7296$ and a bitangential angle $\beta_{Bi}=47.4^\circ$.

The three blades at the center of the cascade are film-cooled while the others serve to provide a periodic outlet flow. Fig. 3 shows the blade geometry and the arrangement of the cooling steam channels. This arrangement enables the supply of steam to single cooling rows. Except for the showerhead (8 rows of holes at the leading edge), all rows can blow out separately.

Pressure probes and thermocouples are installed in the supply channels to enable the cooling steam condition to be determined.

In order to examine the aerodynamic behavior of the

uncooled cascade, the three film-cooled blades were replaced with three solid blades. In addition, a special blade was prepared for measuring the profile pressure distribution at the midspan of the solid blade.

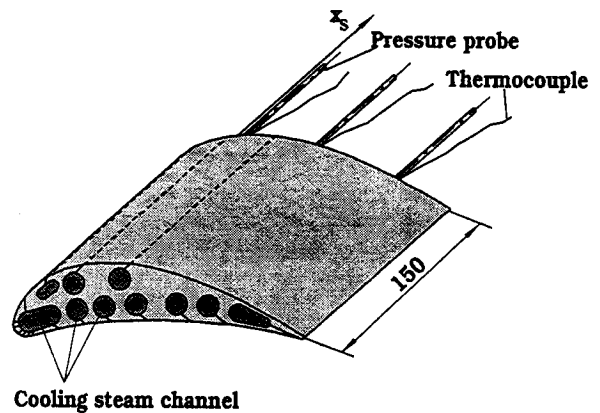


Figure 3: Blade geometry

6 LOSS EVALUATION

Different definitions of the loss caused by the film cooling make it more difficult to compare the results of different examinations, and it is therefore recommended that the definition of the so-called thermodynamic energy loss be used. This definition contains the energy of the main stream as well as the energy of the cooling fluid:

$$\zeta_{th} = 1 - \frac{(1+Y) \cdot \frac{v_2^2}{2}}{\frac{v_{2is}^2}{2} + Y \cdot \frac{v_{c2is}^2}{2}} \quad \text{with: } Y = \frac{\dot{m}_c}{\dot{m}_0} \quad (1)$$

Substitution of the kinetic energy by using the conservation of energy yields the following (see Appendix A):

$$\zeta = 1 - \frac{\left(1 + Y \cdot \frac{c_{pc}}{c_{p0}} \cdot \frac{T_{tc_in}}{T_0}\right) \cdot \left[1 - \left(\frac{p_M}{p_{tM}}\right)^{\theta_M}\right]}{1 - \left(\frac{p_M}{p_{t0}}\right)^{\theta_0} + Y \cdot \frac{c_{pc}}{c_{p0}} \cdot \frac{T_{tc_ex}}{T_0} \cdot \left[1 - \left(\frac{p_M}{p_{tc}}\right)^{\theta_c}\right]} \quad (2)$$

Determination of the experimental loss is performed on the basis of $T_{tc_in} = T_{tc_ex}$. This appears to be well-founded because of the small difference between the main and the coolant steam temperature and the small length-to-diameter ratio of the film holes (≤ 3).

7 PRELIMINARY INVESTIGATION

7.1 Similarity

Experiments on scaled models inevitably give rise to the question as to whether or not the results are comparable to those of full-scale models. The similarity coefficients allow a statement to be made about the similarity between the original and the model flow field. These coefficients arise from the three dimensional

consideration of the flow field (see Remmlinger, 1988):

- conservation of mass
- conservation of momentum
- conservation of energy.

By transforming these equations (for the investigation of the similarity coefficients, the superheated steam is treated as an ideal gas) and observing the geometric conditions, the following similarity coefficients have to be examined.

Aerodynamic coefficients:

- Mach number of main stream
- Reynolds number of main stream $Re_{l_{bl}}$
- Ratio of coolant to main stream momentum
- Coolant-to-mainstream mass flux ratio evaluated at the film hole exit (blowing ratio) or mass flow rate

Thermodynamic coefficients:

- Prandtl number
- Isentropic exponent
- Ratio of temperatures
- Ratio of thermal conductivities
- Ratio of specific heats

$$\pi_T = \frac{T_0 - T_c}{T_0}$$

$$\pi_\lambda = \frac{\lambda_0 - \lambda_c}{\lambda_0}$$

$$\pi_{c_p} = \frac{c_{p0} - c_{pc}}{c_{p0}}$$

The comparison of these similarity coefficients is shown in Table 5 (see Appendix B). While it was possible to vary the Mach number, the ratio of cooling to mainstream momentum and the mass flow rate without any problems, the low experimental Reynolds number ($Re_2 \approx 4 \cdot 10^5$) led to the ratio $\frac{Re_{orig}}{Re_{model}} = 6.6$.

It is, however, possible to use the results yielded by the investigations on the steam test rig. Fig. 4 shows the influence of the Reynolds number on the efficiency (see Dejc et al.). The diagram shows the data for a smooth surface without roughness. The influence of the Reynolds number on the results decreases with increasing roughness. The film cooling holes and coolant jets have the same effect as a rough surface and reduce the influence of the Reynolds number.

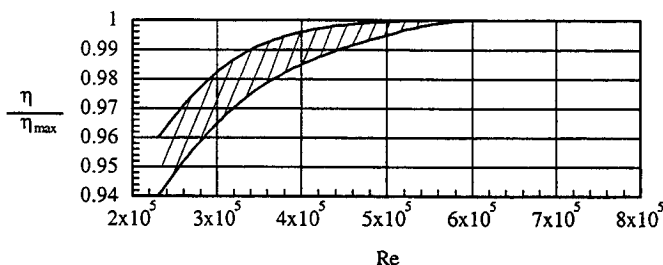


Figure 4: Influence of Reynolds number on relative internal efficiency (Dejc et al.)

The biggest portion of the film-cooling-induced loss is mixing loss. The mixing behavior essentially depends on the flow pattern of the boundary layer, i.e. whether this is laminar or

turbulent. The influence of the Reynolds number on the mixing behavior can be neglected if the boundary layer is turbulent. The showerhead at the leading edge of the investigated turbine causes the boundary layer to change from a laminar flow to turbulent flow, and it is therefore possible to assume that the Reynolds number only has a small influence on the experimental results. Experiments performed with different Reynolds numbers have confirmed this assumption. Furthermore, the numerical code allows the conditions of the experimental investigations to be calculated.

Unfortunately, the thermodynamic coefficients also showed bad agreement. However, the main object of the investigation was to examine the aerodynamic behavior of the film-cooled cascade and not the thermodynamic behavior inside the mixing zone (e.g. local temperature distribution or film-cooling effectiveness).

7.2 Determination of Profile Pressure Distribution

In case of film-cooled blades, the cooling mass flow of each row of holes depends on the ratio between the coolant pressure and the pressure at the exit of the hole determined by the flow field. For this reason it was necessary to establish the profile pressure distribution for the crucial flow parameters (Mach and Reynolds number).

To this end, a special prepared blade with 15 pressure holes on the pressure side and 19 pressure holes on the suction side was manufactured. The pressure distributions were measured at six outlet Mach numbers (Fig. 5) and integrated into the mass flow computation. For Mach numbers between these values, the distribution was linearly interpolated.

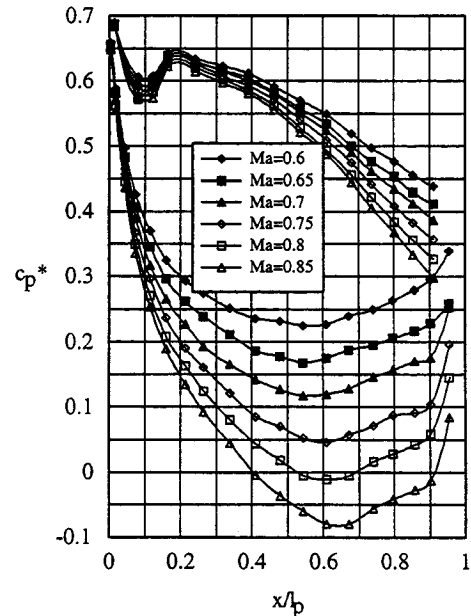


Figure 5: Pressure distribution

With:

$$c_p^* = \frac{p_{pr} - p^*}{p^*} \quad p^* = p_t \cdot P_{crit, Steam}$$

$$P_{crit, Steam} = \frac{p^*}{p_0} = \left(\frac{2}{\gamma + 1} \right)^{\frac{\gamma}{\gamma - 1}}$$

7.3 Investigation of Pressure Loss Correlations of Cooling Steam Supply

In addition to the pressure distribution on the blade it is necessary to know the real exit cooling flow pressure, and for this reason the pressure loss of the cooling flow from the plenum to the exit of the hole was experimentally defined for different cooling steam mass flows. The results of the measurements were converted into pressure loss correlations. The cooling mass flow can then be determined on the basis of these correlations for each row of holes, plenum pressure, inlet flow and Mach number. Fig. 6 gives an example of the reduced mass flow of a suction side row (row SS) and a pressure side row (row PS).

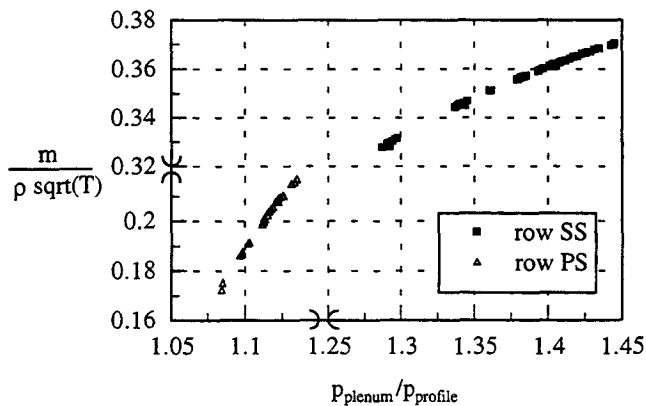


Figure 6: Reduced cooling mass flow

These pressure loss correlations are integrated in the computer-controlled data acquisition and enable a real time coolant mass flow control. The result of the orifice measurement of the coolant flow is compared with the mass flow computed by means of the pressure correlations, and in the event of a discrepancy the control system issues a corresponding signal.

7.4 Thermocouple Installation and Calibration

In order to determine the kinetic loss defined in Equation 2 it is necessary to know the local temperature of the outlet flow. Since the test rig had so far only been used for investigations on uncooled blades it was necessary to widen the outlet 5-hole-wedge type probe with a thermocouple. The difference between the inlet and outlet temperature has a great influence on the result of the kinetic loss. A special calibration procedure was performed in order to minimize the uncertainties.

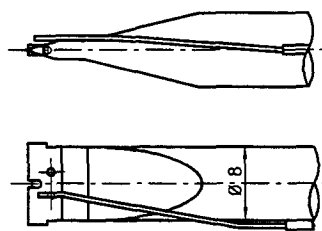


Figure 7: Outlet probe

The thermocouple for the inlet flow and the thermocouple on the probe for the outlet flow were calibrated with a highly precision calibration PT100 sensor element in heated oil. Thus, the standard equation for NiCr-Ni thermocouples was specified for the inlet thermocouple and the outlet thermocouple.

In a second step the recovery factor of the probe thermocouple was determined. This factor depends on the Mach number of the flow as well as on the probe. Because of the asymmetric position of the thermocouple on the probe (s. Fig. 7) it was feared that the measured temperature depended on the angle

of incidence. In the experiments the probe was fixed in the outlet flow and the angle of incidence depends on the outlet flow which means that the recovery factor was determined for different angles of incidence. In an uncooled, adiabatic flow, this calibration procedure led to a maximum temperature difference between the inlet and outlet flow of 0.8K at the test level of 510K (see Urban).

7.5 Experiments at Different Coolant-to-Mainstream Temperature Ratios

In order to confirm the results presented in other papers (Pietrzyk et al.) experiments were performed at different coolant-to-mainstream density ratios. The steam test rig allows the density of the cooling flow to be varied by changing the coolant temperature. The results of this investigation are shown in the following table:

T_c/T_0	ρ_c/ρ_0	Ma_2	mfr/mfr_d	$\beta - \beta_d$	ζ/ζ_d
0.7	1.68	0.75	1.6	-0.08	2.4
0.8	1.47	0.75	1.6	0.03	2.5

Table 2: Results of the density variation

Due to the fact that only an insignificant influence of the density was observed, the temperature ratio of $T_c/T_0=0.8$ was chosen for the main investigation. In order to reduce the temperature ratios it was necessary to either increase the mainstream temperature or to reduce the coolant temperature. The maximum mainstream temperature is 520 K which is determined by the insulating material. The lowest coolant temperature is limited by the steam characteristics. For each pressure there exists a so-called saturation temperature. Below a given saturation temperature, the steam changes from superheated steam to saturated steam (containing droplets), and it is therefore important to maintain the coolant steam temperature above the saturation temperature. During the experiments detailed here, this temperature limit was approximately 360 K.

7.6 Experimental Uncertainties

Uncertainty is always a critical factor in experimental investigations, and the accuracy of the measurements determines the validity of the results. For the investigations performed on the test rig, the following uncertainties can be assumed (see Stanewsky et al. and Urban).

$\beta - \beta_d$:	$\pm 0.1^\circ$
Ma	:	± 0.002
y	:	± 0.1 mm
ζ	:	± 0.08

Table 3: Experimental uncertainties

8 MAIN INVESTIGATIONS

8.1 Test Procedure

The normal test procedure starts with a manual adjustment of flow parameters such as mainflow inlet pressure and temperature, outlet pressure and coolant mass flow and temperature. After reaching a constant flow field the 5-hole probe is traversed through the outlet flow of the cascade. The measuring line is located at the midspan of the blade at half the axial chord

downstream of the trailing edge. The probe is traversed through 1.5 pitches in 36 steps. Because steam is used as the working fluid, the pressure pipes are purged using a special purging mechanism. The data acquisition can only be performed when the pipes are absolutely dry. The purging procedure therefore interrupts the measurement and blows the condensate into the test rig. After closing the purging valves, it is necessary to wait until the pressure has settled at the required level. The signals can be stored when the pressure sensors measure the same undisturbed pressure twice.

8.2 Test Program

The investigation of the film-cooling effects contained an extensive variation of the cooling geometry. Because of the high number of geometric variations the results presented in this paper are reduced to a small fraction which demonstrated the validity of the experiments and also confirms the numerical code. The table below lists the test program.

Mass flow rate	coolant to mainstream temperature	outlet Mach number	rows (see Fig.13)
$mfr/mfr_d = 0$	-----	$0.6 \leq Ma_2 \leq 0.75; \Delta Ma_2 = 0.05$	none
$0.63 \leq mfr/mfr_d \leq 2.6$	$\pi_T = 0.15$	$0.6 \leq Ma_2 \leq 0.75; \Delta Ma_2 = 0.05$	all
$0.52 \leq mfr/mfr_d \leq 1.9$	$\pi_T = 0.15$	$0.7 \leq Ma_2 \leq 0.75; \Delta Ma_2 = 0.05$	TE closed
$0.17 \leq mfr/mfr_d \leq 0.41$	$\pi_T = 0.15$	$0.7 \leq Ma_2 \leq 0.75; \Delta Ma_2 = 0.05$	only TE
$mfr/mfr_d = 0.9$	$\pi_T = 0.15$	$0.7 \leq Ma_2 \leq 0.75; \Delta Ma_2 = 0.05$	PS&TE closed

Table 4: Test program

As explained in Section 7.3 above, the plenum-to-hole exit pressure ratio determines the coolant mass flow of each row (see Fig. 5). While the pressures at the holes exit depend on the main flow Mach number, the pressure of the plenum is adjustable. The variation from full-coverage film cooling to the variations with closed rows at the same plenum pressure is combined with a reduced coolant mass flow. The reduction just contains the mass flow of the closed rows. The mass flow through the open rows and, accordingly, the momentum flux is not affected by the variation. In this way it is possible to separate the influence of the coolant jet location from the influence of the momentum flux.

For the variations with closed rows, the holes are sealed by means of a special high temperature glue which also ensures that the roughness caused by the unused holes is eliminated. The roughness of the closed holes is therefore identical to the roughness of the surfaces.

8.3 Reference Measurements in the Uncooled Cascade

For reference purposes, two different measurements were performed in the uncooled cascade. The measurements were performed on the solid blade without any holes as well as on a drilled blade in order to examine the influence of the holes without blowing out. The results are shown in Fig. 8. The loss values shown are the measured values relative to the value at the design point ($Ma_2=0.75$); the angles are deviations from the design angle. The values shown here are the pitchwise mass-averaged values of

measurements at the midspan of the blade.

Whereas the rough surface of the drilled blade leads to an insignificant smaller outlet angle β , this type of blade also exhibits a significant increase in loss. This is caused by the earlier transition of the boundary layer and the increase in turbulence of the turbulent boundary layer.

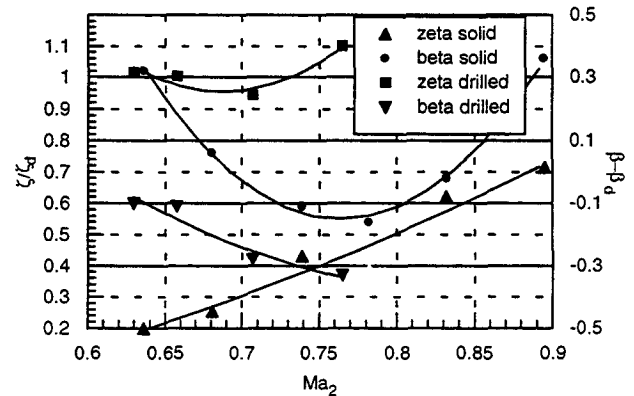


Figure 8: Loss and angle vs. Mach number

By contrast to other investigations (Osnaghi et al.), the geometry of the drilled blade allows these effects to be separated from the effect of the flow through the hollow blade. Because of the fact that each cooling row, except the showerhead, has its own steam channel (Fig. 3) it is impossible for the mainstream to enter the hollow blade and escape through the rows on the suction side or at the trailing edge. The increase in loss is therefore unquestionably based on the two effects explained above.

8.4 Measurements in the Full-coverage Film-cooled Cascade

The results of the investigations of the full-coverage film-cooled cascade are presented in Fig. 9.

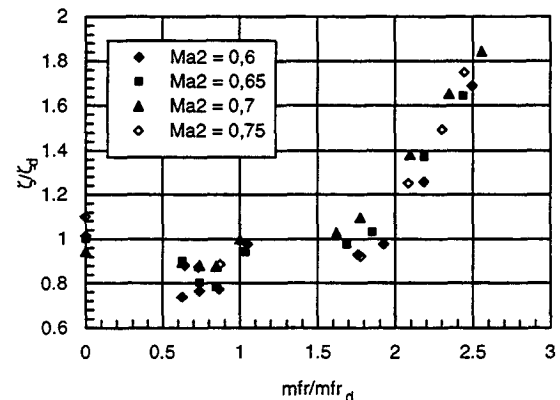


Figure 9: Loss vs. mass flow ratio

The graph clearly shows that the injection of the cooling steam at mass flow ratios below the design point ($mfr/mfr_d=1$) reduces the loss in comparison with the drilled uncooled blade. The uncontrolled circulation of steam through the showerhead (pressure gradients from pressure to suction side) seems to be the reason for the higher loss value at the drilled uncooled blade (see Köllen). Above the value 1.8 times mfr_d , the loss increases very fast. The reason for the sudden increase in loss can be found by examining at the ratio of coolant to mainstream momentum flux (Fig. 10). Because of the fact that the momentum increases

quadratically relative to the cooling stream velocity, a higher mass flow ratio quickly leads to a high ratio of coolant to mainstream momentum flux. This causes a deeper penetration of the cooling jet into the mainstream and a higher disturbance because of the mixing.

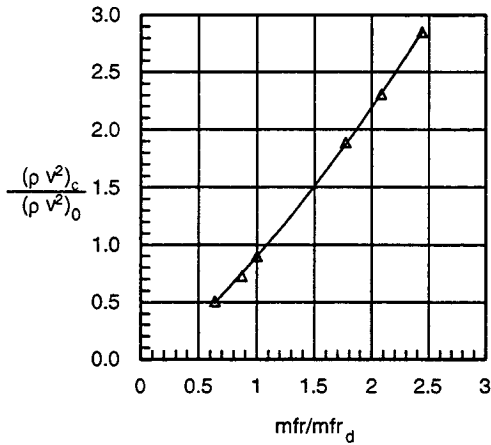


Figure 10: Momentum ratio vs. mass flow ratio

In addition to the averaged values it can be helpful for understanding the flow field to examine the local outlet flow more closely. Fig. 11 shows the reduced local pressure loss and Fig. 12 the local deviations from the design outlet angle at $Ma_2=0.75$.

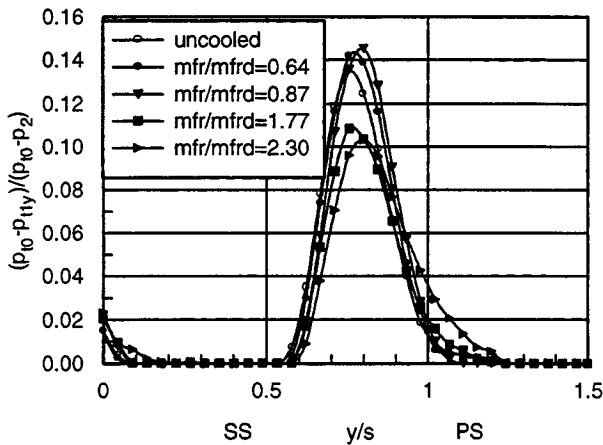


Figure 11: Reduced local total pressure loss

The local reduced total pressure loss increases moderately at first because of the cooling steam. Moreover the wake shifts because of the change in outlet angle. At a mass flow ratio $mfr/mfr_d=1.8$, the behavior reverses and the pressure loss decreases in comparison with the uncooled blade. Above this value the wake energizing effect of the cooling stream and the reduction of the base loss by increasing the base pressure exceed the mixing loss. In addition, the wake widens because of the thicker boundary layer.

A comparison of the local outlet angle deviations shows that the differences between the different mass flow ratios are very small. The main influence of the cooling steam is noticeable in areas close to the suction and pressure sides of the blade. Although the injected steam causes a shift of the outlet flow in general, a real change of the trend only is visible in the area near the blade.

The change in the angle on the pressure side is particularly pronounced.

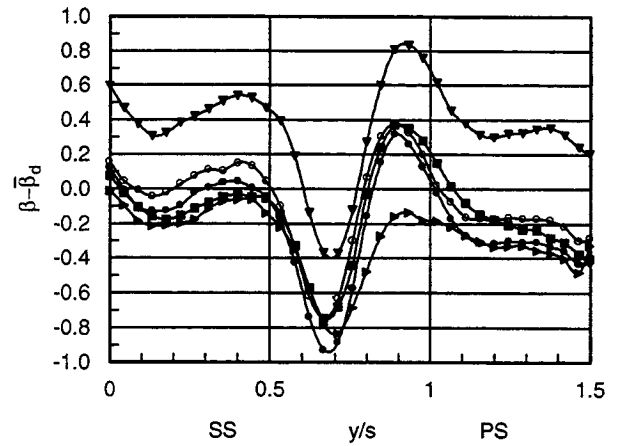


Figure 12: Local deviations from the design outlet angle

The investigation of the cooling mass flow distribution helped find the reason for this pronounced change in angle. The mass flow of each row was computed on the basis of the correlations mentioned above, and charted in Fig. 14. Fig. 13 shows the abbreviations used for the rows.

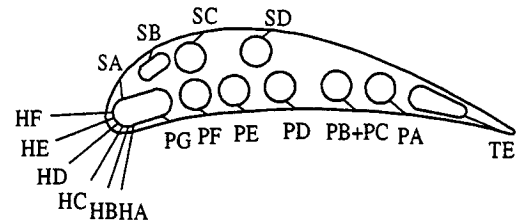


Fig. 13: Abbreviations

The percentage cooling steam mass flow of the showerhead (rows HA-SA) and the pressure side rows PD-PG increases in proportion to the increase in the mass flow ratio whereas the percentage mass flow of the suction side rows (SB-SD), the trailing edge (TE) and the rows PA-PC decreases considerably.

The reason for the different behavior of the rows is the different pressure loss across the steam channels. Thus the over-proportional increase in cooling mass flows on the pressure side brings about the over-proportional local outlet flow reduction on the pressure side.

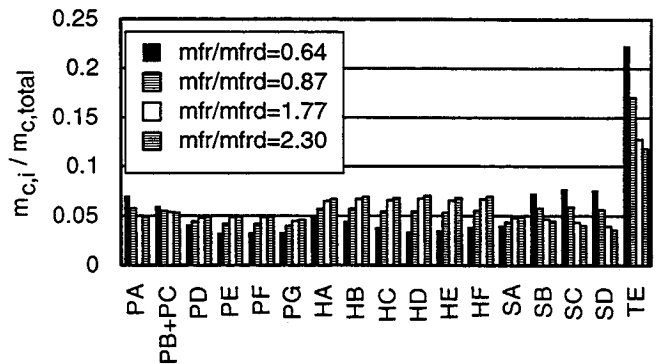


Figure 14: Distribution of the cooling steam ($Ma_2=0.75$)

8.5 Measurements at the Film-cooled Blade with TE-variations

The influence of the trailing edge was investigated by experiment on a completely cooled blade with closed trailing edge and on an undrilled blade and where only the trailing edge was cooled. Fig. 15 shows the loss term of the TE closed blade in comparison with a full-coverage cooled blade at the design Mach number.

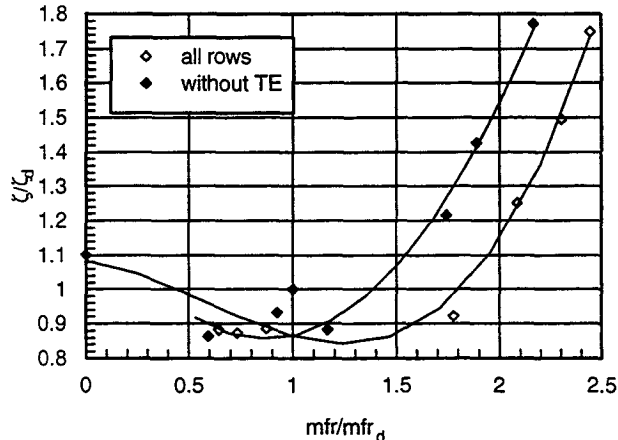


Figure 15: Comparison of the TE closed blade loss terms

It is obvious that the trailing edge flow has a positive effect on the loss behavior. With the full-coverage cooled blade nearly the same loss values are reached at a higher mass flow rate. This means that the loss increases more slowly with the full-coverage cooled blade than with the TE closed blade.

Fig. 16 shows the local outlet angle deviation of the TE closed blade. The absence of the pressure-side trailing edge flow leads to a considerable increase in the outlet angle. It can also be seen that the increase in mass flow rate mainly influences the outlet angle in the area near the pressure side (cf. the mass flow distribution in Fig. 14).

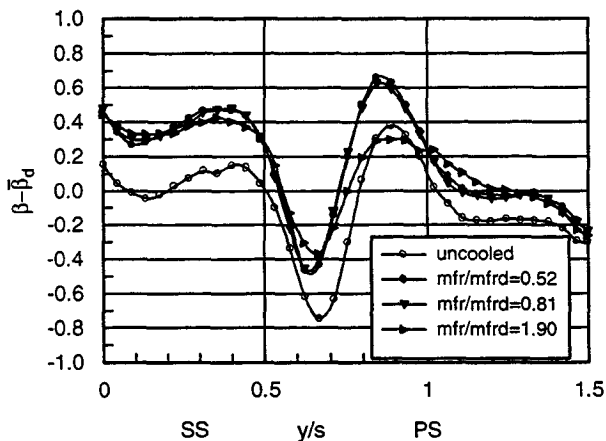


Figure 16: Comparison of the TE closed blade deviations from the design outlet angle ($Ma_2=0.75$)

As the only trailing-edge cooled variant exhibits a very low mass flow rate it is compared in this paper to the solid blade. It is however still possible to link these results with those mentioned above.

Fig. 17 shows the development of the loss term with an increasing mass flow rate at $Ma_2=0.75$. The loss produced by the

trailing-edge cooling flow is generally lower than the loss of the full-coverage cooled blade.

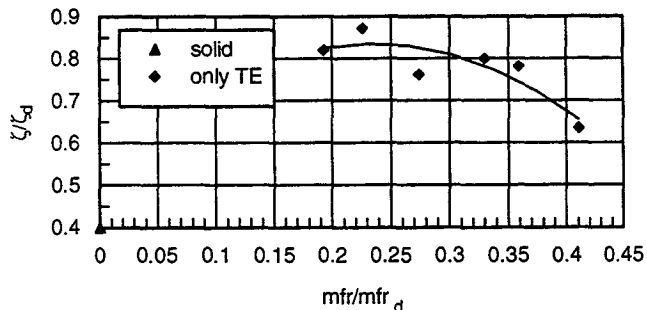


Figure 17: Loss terms of the undrilled TE cooled blade

The decreasing loss with rising coolant flow is caused by the wake energizing effect of the TE flow. This effect exceeds the mixing loss.

8.6 Measurements on the showerhead and suction side cooled blade

Unlike the pressure side, the suction side is very sensitive with regard to flow disturbances. For this reason, minimizing the cooling flow on the suction side is a major objective. Fig. 13 shows that the investigated blade is equipped with only four rows on the suction side, six rows to serve as showerhead and six rows on the pressure side. The mass contribution of the suction side is, as shown in Fig. 14, really small. However, the influence of this mass flow is more pronounced than that of the pressure side mass flow. Table 5 compares the loss terms of the two configurations at $Ma_2=0.75$. The lacking pressure side cooling flow brings about a small decrease of the loss term. Compared to the reduction of the cooling mass (ratio of cooling mass SH+SS cooled to full coverage cooled: 0.7) the reduction in loss is very low. This result reiterates the sensitivity of the suction side flow with regard to disturbances by the cooling flow and the large contribution of the showerhead to the loss production.

	Ma_2	mfr/mfr_d	ζ/ζ_d
SH+SS	0.75	1.25	0.8
full coverage	0.75	1.77	0.92

Table 5 : Loss term of the SH+SS cooled blade

9 SIMPLE CALCULATION METHOD OF IMPULSE MIXING LOSSES

Based on the measurements detailed in the previous section, a simplified method for the calculation of impulse mixing losses was developed and validated. The method utilized for the calculations was based on the prediction model „TOTLOS“ by Hartsel. Hartsel's modeling technique divides the mainflow into two components. One component contains the isentropic expansion from the inlet to the outlet of the blade row, and the second models the massflow around the airfoil. It is the second component that includes the coolant air flow. The impulse mixing of the mainflow and coolant is then solved for each film row. The inviscid momentum equation in the streamwise direction is used under the assumption that the static pressure is constant over the mixing process for each film cooling row. The momentum of the cooling air flow orthogonal to the streamwise direction dissipates,

and so represents the impulse mixing losses of the cooling air flow. After all cooling air flows are injected into the mixing layer of the mainflow a final mixing of the isentropic mainflow and the mixing layer takes place downstream the blade row. This yields the impulse mixing losses for the cooling air flows in the form of equation (1). A detailed description of the numerical solution is given in Appendix C.

Hartsel's model has been used successfully by many other experimenters (Köllen, Ito et. al.). In most of these previous cases, only a single film cooling row ejection has been investigated. The objective of this study was to validate the technique also for multi film cooling row ejection. In order to allow a comparison with the measurements, the case without trailing edge ejection was chosen. The reason for this is the different influence on the flow of the trailing edge injection and airfoil ejection. The simple Hartsel model does not allow to take into account the positive effects of the trailing edge ejection on the trailing edge losses as discussed in Section 8.5 above.

Fig. 18 shows the comparison between the experimental and analytical calculations for the case of a full-coverage film-cooled blade without trailing edge ejection. For a comparison of the measured loss coefficients with the calculated loss coefficients, the measured losses are reduced with the profile loss in the case without cooling air ejection. Therefore, the curves represent only the impulse mixing losses of the blade. For small ejection rates, the model predicts the losses very well. However, for greater cooling air massflows the differences between analysis and experiment increase. For larger massflow rates the cooling air blows out of the boundary layer of the profile, and the situation of the mixing process changes completely. The result is a dramatic increase in mixing losses. The simplified prediction method used in this study is not able to take into account these changes in the flow field. A correction factor must be found to incorporate the effects of cooling flow blowing out of the boundary layer.

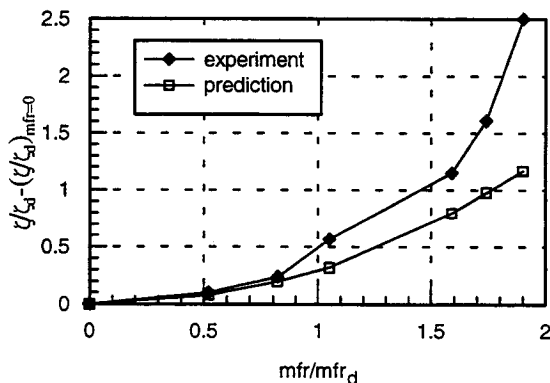


Figure 18: Comparison of measurement with results of analytical calculation(exit Machnumber of $\text{Ma}=0,75$)

However, for massflow rates of the cooling air, which are of interest in terms of real-life applications, the presented method predicts good results. The conclusion of the study is that the presented method of mixing loss calculation can be used for predicting the mixing losses of cooling air during the design phase of a turbine. The predicted losses can be used in the flow calculation of turbines with cooling air flow in addition to the aerodynamic loss correlations (for example Ainley Mathieson, Traupel, et al.).

10 CONCLUSIONS

This paper has presented aerodynamic loss measurements in the presence of film cooling carried out on a cascade steam test rig. It also looked at a simple calculation method based on Hartsel's „TOTLOS“ model adapted to the problem of multi-row film cooling and compared the numerical predictions with experimental results. This allows the following conclusions:

- The comparison of the non-dimensional similarity shows that investigations of film cooling effects can be performed on a steam test rig. The advantage of steam as working fluid and coolant is that it is possible to vary the coolant to mainstream density ratio without using different flow media (e.g. CO_2 as coolant medium). The results of the experiments performed at different density ratios did not show a significant influence of this parameter.
- The design of the blade enabled investigations of different coolant injection locations. Multi-row film cooling as well as single row cooling was performed. The results of these experiments show that coolant ejection on the suction side has a large influence on the aerodynamic behavior and increases the aerodynamic loss very rapidly. The coolant ejection on the pressure side influences the aerodynamic loss only little. The effect of coolant ejection at the trailing edge is positive. The energizing effect of the coolant flow reduces the loss of the film cooled blade.
- The investigation of the local outlet flow field shows that the influence of the coolant flow is concentrated near the blade surface. This result confirms Hartsel's mixing model of an isentropic core flow and a mixing layer.
- The presented calculation method was successfully validated by measurements of a blade with multi-row air ejection. The agreement between the numerical calculated losses and the measurements is good with regard to cooling air massflow typically associated with gas turbines. For cases with high mass flow rates the prediction yields insufficiently low impulse mixing losses. Furthermore the method is not able to predict the losses of a blade with trailing edge ejection. Improving the calculation method to take into account the influence of trailing edge ejection on the aerodynamic loss combined with the trailing edge itself will be one of the main tasks for the future.

11 ACKNOWLEDGEMENTS

The present work has been sponsored by BMBF under the code number 0326820C.

12 REFERENCES

- Ainley, D.G.; Mathieson, G.C.R.: „A Method of Performance Estimation for Axial Flow Turbines“. British ARC, Reports and Memoranda No. 2974, 1951
- Dejc, Trojanovskij, 1973, „Untersuchung und Berechnung axialer Turbinenstufen,“ VEB Verlag Technik Berlin.
- Haller, B.R., Camus, J.-J., 1984, „Aerodynamic loss penalty produced by film cooling transonic turbine blades,“ ASME, Vol.106.
- Ito, S., Eckert, E.R.G., Goldstein, R. J., 1980, „Aerodynamic loss in a gas turbine stage with film cooling,“ ASME, Vol. 102.

Köllen, O., 1986, „Experimentelle und theoretische Analyse der aerodynamischen Verluste in filmgekühlten Turbinenschaufeln,“ Diss. RWTH Aachen.

Day, C.R.B., Oldfield M.L.G., Lock, G.D., 1997, „The Influence of Film Cooling on the Efficiency of an Annular Nozzle Guide Vane Cascade,“ ASME paper 97-GT-521.

Osnaghi, C., Perdichizzi, A., Savini, M., Harasgama, P., Lutum, E., 1997, „The influence of film-cooling on the aerodynamic of a turbine nozzle guide vane,“ ASME paper 97-GT-522.

Parvizinia, M., 1996, „Einfluß der Filmkühlung auf die Aerodynamik von Turbinenschaufeln,“ Diss. RWTH Aachen.

Pietrzyk, J.R., Bogard, D.G., Crawford, M. E., 1990, „Effects of density ratio on the hydrodynamics of film cooling,“ ASME Journal of Turbomachinery, Vol. 112.

Remmlinger, U., 1988, „Die Vorhersage der Filmkühlwirkung bei Gasturbinenschaufeln aus Messungen in einem Heißwindkanal mit Triebwerksähnlichkeit unter Berücksichtigung des Einflusses variabler Stoffwerte,“ Diss. TH Darmstadt.

Stanewsky, E., Kost, F., 1988, „Eichung der Keilsonde KWU3 und Reduktion der Eichdaten“, DFVLR, Aerodynamische Versuchsanstalt Göttingen, IB222-88 C17.

Traupel, W., Thermische Turbomaschinen. 3 Aufl. Band I, Berlin, Springer 1977.

Urban, M., „Experimentelle Untersuchung an gekühlten Gasturbinenschaufeln zum Einfluß der Kühlluftströmung auf den Wirkungsgrad“ RWTH Aachen.

13 APPENDIX A

The loss calculations are based on the following equation defined by Traupel:

$$\zeta_{th} = 1 - \frac{(1+Y) \cdot \frac{v_2^2}{2}}{\frac{v_{2is}^2}{2} + Y \cdot \frac{v_{c2is}^2}{2}} \quad \text{with: } Y = \frac{\dot{m}_c}{\dot{m}_0} \quad (1)$$

By means of Fig. 19, the kinetic loss can be expressed in the general equation 3:

$$\zeta_{th} = 1 - \frac{(\dot{m}_0 + \dot{m}_c) \cdot (h_{t(T_{tM}, k_M)} - h_{(T_M, k_M)})}{\dot{m}_0 \cdot (h_{t(T_{t0}, k_0)} - h_{(T_{0is}, k_0)}) + \dot{m}_c \cdot (h_{t(T_{tc_ex}, k_c)} - h_{(T_{cis}, k_c)})}$$

where: $h, h=f(T, T, k_c, k_0)$.

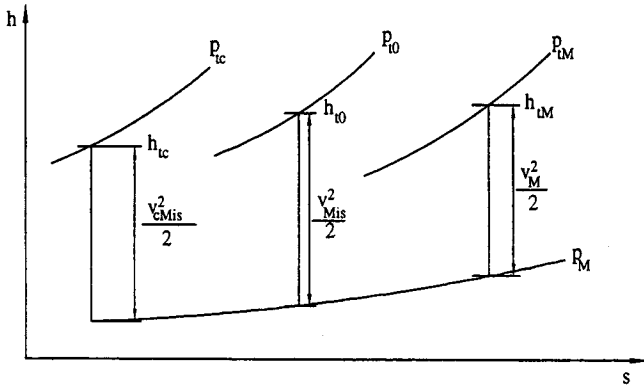


Figure 19: h-s diagram for film cooling

Assuming a constant gas composition of coolant and hot gas equation 3 leads:

$$\zeta_{th} = 1 - \frac{(\dot{m}_0 + \dot{m}_c) \cdot (h_{t(T_{tM})} - h_{(T_M)})}{\dot{m}_0 \cdot (h_{t(T_{t0})} - h_{(T_{0is})}) + \dot{m}_c \cdot (h_{t(T_{tc_ex})} - h_{(T_{cis})})} \quad (4)$$

With superheated steam as an ideal gas and $c_p = f\left(\frac{T+T_t}{2}\right)$:

$$h_t - h = \frac{1}{2} \cdot v^2 = c_p \cdot T_t \left[1 - \left(\frac{p}{p_t} \right)^{\frac{\gamma-1}{\gamma}} \right] \quad \text{and } \frac{\gamma-1}{\gamma} = \theta \quad (5)$$

equation 4 can be written as:

$$\zeta_{th} = 1 - \frac{(\dot{m}_0 + \dot{m}_c) \cdot c_{pM} \cdot T_{tM} \cdot \left[1 - \left(\frac{p_M}{p_{tM}} \right)^{\theta_M} \right]}{\dot{m}_0 \cdot c_{p0} \cdot T_{t0} \cdot \left[1 - \left(\frac{p_0}{p_{t0}} \right)^{\theta_0} \right] + \dot{m}_c \cdot c_{pc} \cdot T_{tc_ex} \cdot \left[1 - \left(\frac{p_M}{p_{tc}} \right)^{\theta_c} \right]} \quad (6)$$

To obtain the unknown temperature T_{tM} it is necessary to examine the energy balance of the mixing model system and the blade system more closely (Fig. 20):

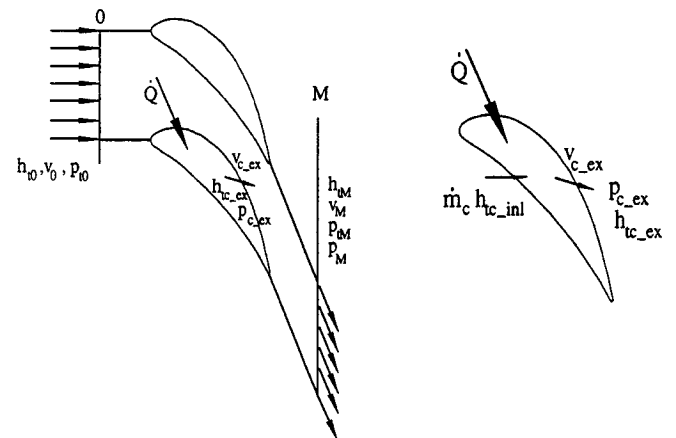


Figure 20: Energy balance of mixing model system and blade system

The conservation of energy for the mixing model system and the blade system can be written as:

Mixing model system:

$$\dot{m}_0 \cdot h_{t0} + \dot{m}_c \cdot h_{tc_ex} = \dot{Q} + (\dot{m}_0 + \dot{m}_c) \cdot h_{tM} \quad (7a)$$

Blade system:

$$\dot{m}_c \cdot h_{tc_inl} + \dot{Q} = \dot{m}_c \cdot h_{tc_ex} \quad (7b)$$

Elimination of \dot{Q} and $h = c_p \cdot T$ yields the unknown temperature T_{tM} :

$$T_{tM} = \frac{\dot{m}_0 \cdot c_{p0} \cdot T_{t0} + \dot{m}_c \cdot c_{pc_int} \cdot T_{tc_int}}{c_{pM} \cdot (\dot{m}_0 + \dot{m}_c)} \quad (8)$$

Thus equation 6 can be rewritten as follows:

$$\zeta_{th} = 1 - \frac{(\dot{m}_0 \cdot c_{p0} \cdot T_{t0} + \dot{m}_c \cdot c_{pc} \cdot T_{tc_int}) \cdot \left[1 - \left(\frac{p_M}{p_{t0}} \right)^{\theta_M} \right]}{\dot{m}_0 \cdot c_{p0} \cdot T_{t0} \cdot \left[1 - \left(\frac{p_M}{p_{t0}} \right)^{\theta_0} \right] + \dot{m}_c \cdot c_{pc} \cdot T_{tc_ex} \cdot \left[1 - \left(\frac{p_M}{p_{tc}} \right)^{\theta_c} \right]} \quad (9)$$

or

$$\zeta = 1 - \frac{\left(1 + Y \cdot \frac{c_{pc}}{c_{p0}} \cdot \frac{T_{tc_int}}{T_{t0}} \right) \cdot \left[1 - \left(\frac{p_M}{p_{tM}} \right)^{\theta_M} \right]}{1 - \left(\frac{p_M}{p_{t0}} \right)^{\theta_0} + Y \cdot \frac{c_{pc}}{c_{p0}} \cdot \frac{T_{tc_ex}}{T_{t0}} \cdot \left[1 - \left(\frac{p_M}{p_{tc}} \right)^{\theta_c} \right]} \quad (2)$$

For determining the mixed-out plane M values it is necessary to mix out the measured flowfield of plane 1 to the mathematically equivalent flow of plane M (see Fig. 21).

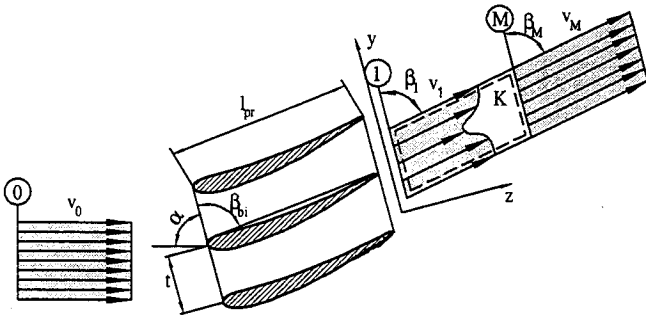


Figure 21: Schematic of the mixing out process

The flow field in plane M is equivalent to the flow field in plane 1 with regard to mass, energy and momentum. The mixing-out process is thus essentially an averaging process. The conservation equations for determining the flow field of plane M are:

Conservation of mass in the direction of z:

$$I_1 = \frac{V_M}{V_{yM}} \cdot \sin \beta_M = \frac{1}{t} \int_0^t \left[\frac{v_1(y)}{v_{y1}(y)} \cdot \sin \beta_1(y) \right] \cdot dy \quad (10)$$

Conservation of momentum in the direction of z:

$$I_2 = \frac{V_M^2}{V_{y1}(y)} \cdot \sin \beta_M + p_M = \frac{1}{t} \int_0^t \left[\frac{v_1^2(y)}{v_{y1}(y)} \cdot \sin^2 \beta_1(y) + p_1(y) \right] \cdot dy \quad (11)$$

Conservation of momentum in the direction of y:

$$I_3 = \frac{v_1^2(y)}{v_{y1}(y)} \cdot \sin \beta_M \cdot \cos \beta_M = \frac{1}{t} \int_0^t \left[\frac{v_1^2(y)}{v_{y1}(y)} \cdot \sin \beta_M(y) \cdot \cos \beta_M \right] \cdot dy \quad (12)$$

Constancy of energy:

$$E = \left(c_{pM} \cdot T_{t1} + h_{0M} \right) \cdot \frac{V_M}{V_{yM}} \cdot \sin \alpha_M = \frac{1}{t} \int_0^t \left(c_{p1}(y) \cdot T_{t1}(y) + h_{01}(y) \right) \cdot \frac{V_M}{V_{yM}} \cdot \sin \alpha_1(y) \cdot dy \quad (13)$$

with h , h , and $v=f(p,t)$.

14 APPENDIX B

Table 6 lists the non-dimensional similarity coefficients.

Mach number of mainstream	$0.8 \leq \frac{Ma_{model}}{Ma_{orig}} \leq 1.2$
Reynolds number Re_{1bi}	$\frac{Re_{model}}{Re_{orig}} = 0.15$
Ratio of cooling to mainstream momentum	$0.5 \leq \frac{I_{model}}{I_{orig}} \leq 2.9$
Mass flow rate	$0 \leq \frac{mfr}{mfr_d} \leq 2.5$
Prandtl number	$\frac{Pr_{model}}{Pr_{orig}} = 0.89$
Ratio of isentropic exponents	$\frac{\gamma_{model}}{\gamma_{orig}} = 1.008$
Ratio of temperatures	$0.15 \leq \frac{(\pi_T)_{model}}{(\pi_T)_{orig}} \leq 0.3$
Ratio of thermal conductivities	$\frac{(\pi_\lambda)_{model}}{(\pi_\lambda)_{orig}} = 0.86$
Ratio of specific heats	$\frac{(\pi_{c_p})_{model}}{(\pi_{c_p})_{orig}} = 2.54$

Table 6: Comparison of non-dimensional similarity coefficients

15 APPENDIX C

15.1 Mixing of cooling air in the mixing layer

In order to simplify the conservation equations listed below the assumption is made that during the injection of each film cooling row into the mixing layer the static pressure remains constant. For the boundary found in Fig. 22 the conservation equations are then reduced to the following form:

Conservation equation of massflow:

$$\rho_0 \cdot v_0 \cdot F_0 + \rho_c \cdot v_c \cdot F_c = \rho_m \cdot v_m \cdot F_m \quad (14a)$$

Momentum conservation in streamwise direction:

$$\rho_0 \cdot v_0^2 \cdot F_0 + \rho_c \cdot v_c^2 \cdot F_c \cdot \cos \alpha_c = \rho_m \cdot v_m^2 \cdot F_m \quad (14b)$$

Conservation of energy:

$$\rho_0 \cdot v_0 \cdot F_0 \cdot h_{t0} + \rho_c \cdot v_c \cdot F_c \cdot h_{tc} = \rho_m \cdot v_m \cdot F_m \cdot h_{tm} \quad (14c)$$

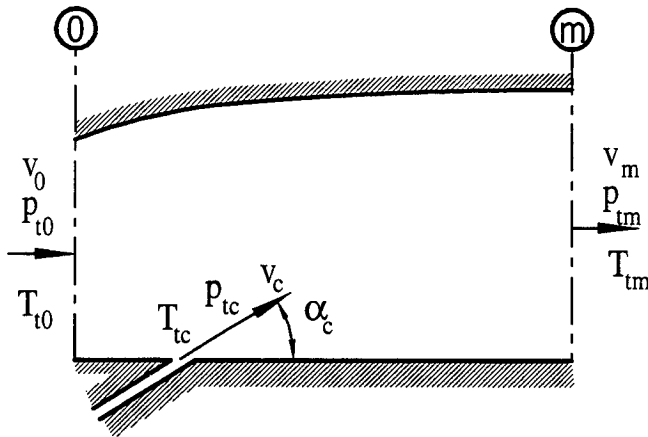


Figure 22: Boundary for cooling air flow with the mixing layer

Because of the assumption, that the static pressure remains constant during the mixing process, the pressure forces cancel each other out in the momentum equation listed above. All variables on the left side of the equations are known, so that with the three equations (14a-14c) the three unknown variables on the right hand side can be calculated. Note that for the direction orthogonal to the flow, the momentum of the cooling air flow dissipates, and that therefore there is no momentum flux of the mixed flow in plane m for this direction.

15.2 Mixing of core flow and mixing layer

The definition of the mainflow and the mixing layer are found in Fig. 23. There you can see the definition of the mainflow and the mixing layer. The factor σ gives the massflow for the mixing layer as a fraction of the inlet mass flow in plane 0. The value σ has a small impact on the predicted losses; so one should choose a constant value for the mixing layer thickness. The presented calculations here are done with a constant value of $\sigma=0,1$ for the pressure and the suction side. In plane 1 all cooling flows are injected into mixing layer. For the final mixing process of the mixing layer and the isentropic core from plane 1 to plane M the equations 14a - 14c are used.

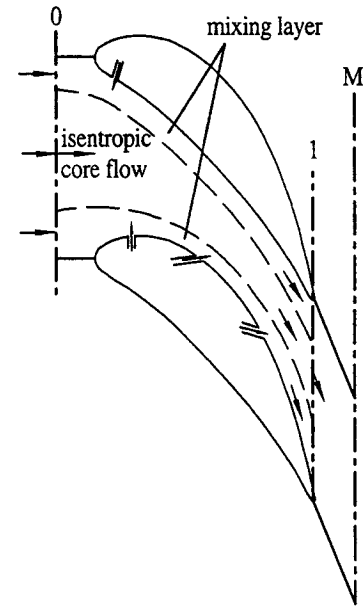


Figure 23: Boundary for the mixing loss calculation

For the final mixing process the inviscid conservation equations are used between plane 1 and plane M. The final result is the average mixing loss for the total mainflow. The conservation equations for the mixing process are as follows:

Conservation of mass flow

$$\dot{m}_0 \cdot (1 - \sigma) + \sigma \cdot \dot{m}_0 + \dot{m}_c = \rho_M \cdot v_M \cdot F_M \cdot \sin \beta_M \quad (15a)$$

Momentum equation in axial direction:

$$\dot{m}_0 (1 - \sigma) \sin \beta_1 v_{1is} + (\sigma \dot{m}_0 + \dot{m}_c) \sin \beta_1 v_m + p_1 F_1 = \quad (15b)$$

$$\dot{m}_M v_M \sin \beta_M + p_M F_M$$

Momentum equation in circumferential direction:

$$\dot{m}_0 (1 - \sigma) \cos \beta_1 \cdot v_{1is} + (\sigma \dot{m}_0 + \dot{m}_c) \cos \beta_1 \cdot v_m = \quad (15c)$$

$$\dot{m}_M v_M \cos \beta_M$$

Energy equation:

$$\dot{m}_0 \cdot (1 - \sigma) \cdot h_{t0} + (\sigma \cdot \dot{m}_0 + \dot{m}_c) \cdot h_{tm} = \rho_M \cdot v_M \cdot F_M \cdot h_{tM} \quad (15d)$$

Under the additional assumption that area F_1 is equal to area F_M , the equation system 15a-15d can be solved. With the known variables on the left side of the equations the unknown properties (density, flow angle, velocity, total enthalpy) in plane M can be calculated. It is thus possible to predict the loss coefficient for the mixing loss following equation 16:

$$\zeta_{th} = 1 - \frac{(1 + Y) \cdot \frac{v_M^2}{2}}{\frac{v_1^2}{2} + Y \cdot \frac{v_{c1is}^2}{2}} \quad \text{with } Y = \frac{\dot{m}_c}{\dot{m}_0} \quad (16)$$